# Supplementary Information for *Soft Matter*

## Gecko-Inspired Bidirectional Double-Sided Adhesives

*Zhengzhi Wang, Ping Gu and Xiaoping Wu*

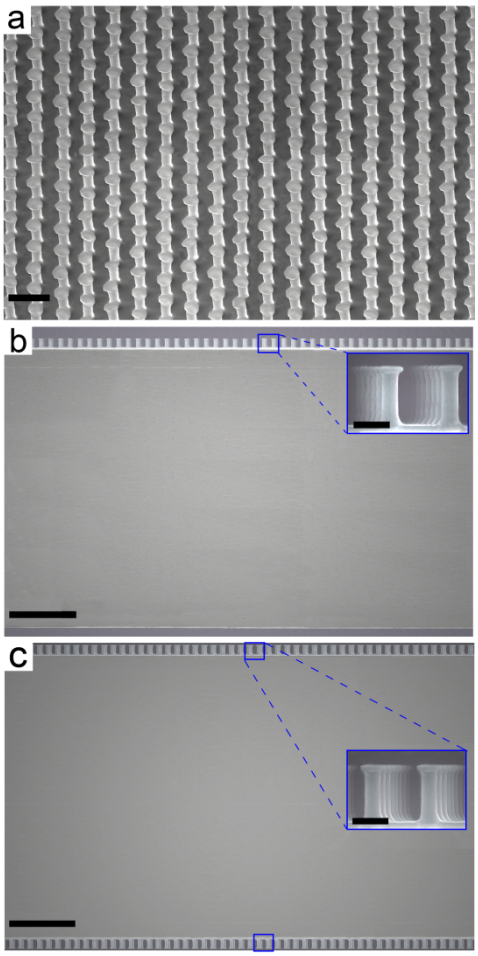


**Fig. S1** SEM images of the control samples with vertical PUA pillars from (a) top view, and side views of (b) single-sided, (c) double-sided adhesive. Scale bars are 10 μm, 50 μm (5 μm), and 50 μm (5 μm) for the image (inset) from (a) to (c), respectively.

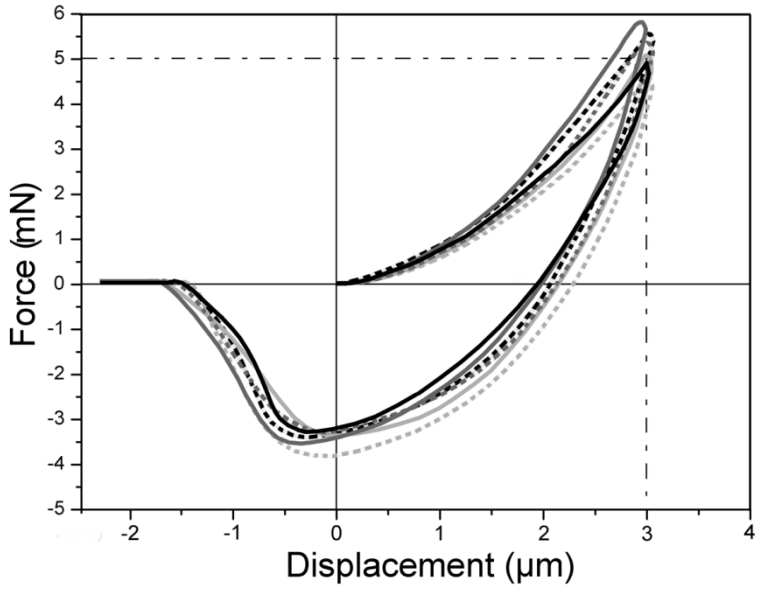


**Fig. S2** Load-displacement curves of the SSA indentation (or load-pull) tests for determining proper value of the preload used in the L-D-P tests, showing ~ 3 μm normal displacement needs ~ 5 mN normal preload.

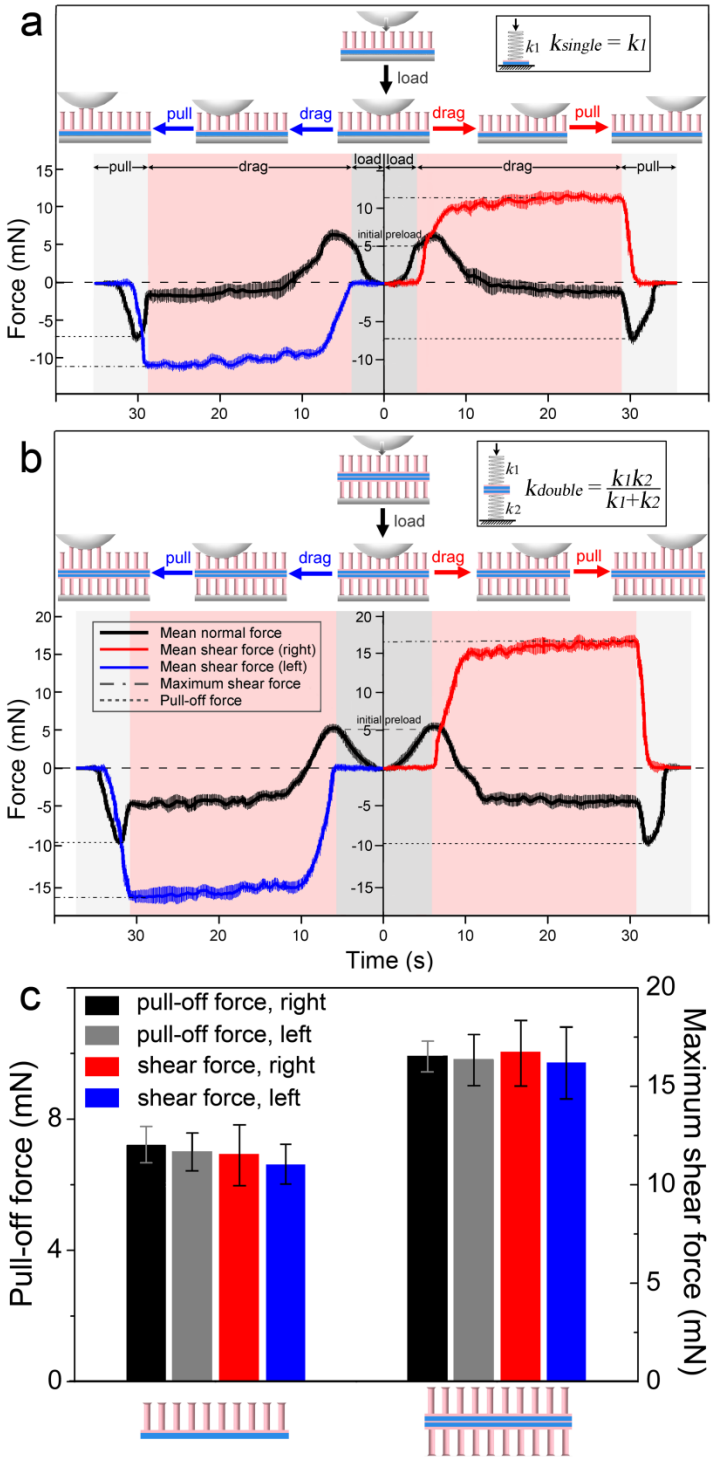


**Fig. S3** Illustrations and real-time plots of the normal and shear forces during L-D-P tests of (a) single-sided and (b) double-sided control sample. Plot layouts are the same as Fig. 2. Upper right insets illustrute the effective spring-in-series model for the double-sided patterned pillars. (c) Pull-off force and maximum shear force at the two directions (right and left) extracted from the real-time plots, showing isotropic adhesive bahaviors of the vertical pillar samples.

**Text S1:** Peeling moment caused by tip/fiber relative rotation during L-D-P process

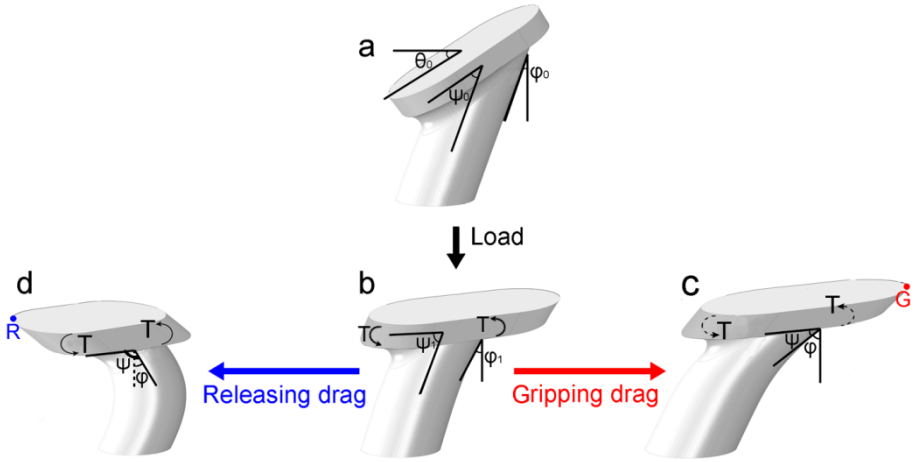


**Fig. S4** Illustration of the tip/fiber peeling moment during the L-D-P test. Tip angle $\theta$, fiber angle $\varphi$, and tip/fiber intersection angle $\psi$ are defined in the side-view illustration of each experimental stage. (a) Natural geometry of the pillar. Deformed pillar after (b) normal preloading, (c) gripping dragging, and (d) releasing dragging. Peeling moment (or internal deformation-resistance) caused by the tip/fiber relative rotation is denoted by $T$. The two points (point G in (c) and point R in (d)) indicate the leading edges, from where the detachment might be initiated during dragging.

Assuming isotropic material and small deformation, the peeling moment should be proportional to the level of tip/fiber relative rotation:

$$T = G \cdot \Delta\psi \tag{S1}$$

where $G$ is unit rotation strength, which is related to material rigidity and tip/fiber interface strength. The symbol '$\Delta$' denotes angle change with respect to the undeformed value. According to the geometrical illustrations shown in Fig. S4, the tip angle disappears while the fiber angle and tip/fiber intersection angle increase to a certain value ($\varphi_1$ and $\psi_1$) after the normal preloading (Fig. S4b). For the following gripping dragging (Fig. S4c),

$$\Delta\varphi = \varphi - \varphi_0 \ , \ \psi = \frac{\pi}{2} - \varphi \tag{S2}$$

$$\Delta\psi = \psi - \psi_0 = (\frac{\pi}{2} - \varphi) - (\frac{\pi}{2} - (\theta_0 + \varphi_0)) = \theta_0 - \Delta\varphi \tag{S3}$$

while for the releasing dragging (Fig. S4d),

$$\Delta\varphi = \varphi + \varphi_0 \ , \ \psi = \frac{\pi}{2} + \varphi \tag{S4}$$

$$\Delta\psi = \psi - \psi_0 = (\frac{\pi}{2} + \Delta\varphi - \varphi_0) - (\frac{\pi}{2} - (\theta_0 + \varphi_0)) = \theta_0 + \Delta\varphi \tag{S5}$$

Accordingly, the peeling moment becomes smaller and smaller during gripping dragging and reaches zero when the change of fiber angle ($\Delta\varphi$) equals to the original tip angle $\theta_0$, at which point the tip can obtain full contact with the indenter. By contrast, the peeling moment keeps increasing during releasing dragging which results in early detachment of the tip from the leading edge (point R in Fig. S4d).

**Text S2:** Finite element modeling (FEM) of a single pillar during L-D-P process

The dual-angled PUA pillar and a rigid flat indenter were constructed using the commercially available software: Abaqus/CAE v6.12-1.[S1] The L-D-P processes were analyzed by the Abaqus/Standard solver. The movement of the indenter was kept consistent with the one used in the tests except that all the movements in the simulation were displacement-controlled. Coulomb friction was assumed for the interaction between the indenter and the fiber with a constant coefficient of 0.3. The adhesion behavior was simulated by using the effective spring models as introduced in our previous work.[S2]

Fig. S5 shows the von Mises stress contours of the pillar at the end of each experimental stage, indicating qualitative agreements between the simulations and experiments. Full contact between the tip and the indenter and uniformly distributed stress at the indenter/tip interface can be obtained for dragging and pulling off along the gripping direction. Consistent with the experimental observations, the pillar shows high stretchability during the retraction of the indenter, which indicates favorable adhesion performance. By contrast, early detachment of the tip from the leading edge occurs; and obvious stress concentrations can be observed at the tip/indenter interface due to the gradually increased peeling moment for dragging and pulling off along the releasing direction.

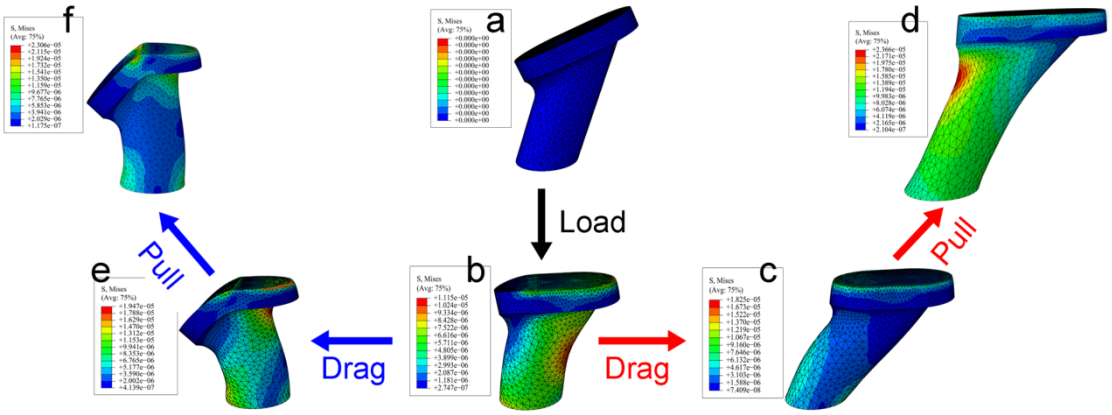


**Fig. S5** Results of FEM. Pillar deformation and von Mises stress distribution are shown at the end of each experimental stage: (a) initial unloaded state, (b) normal preloading, (c) gripping dragging, (d) pulling-off in the gripping direction, (e) releasing dragging, and (f) pulling-off in the releasing direction. For better visualization, the indenter is removed in the contours.

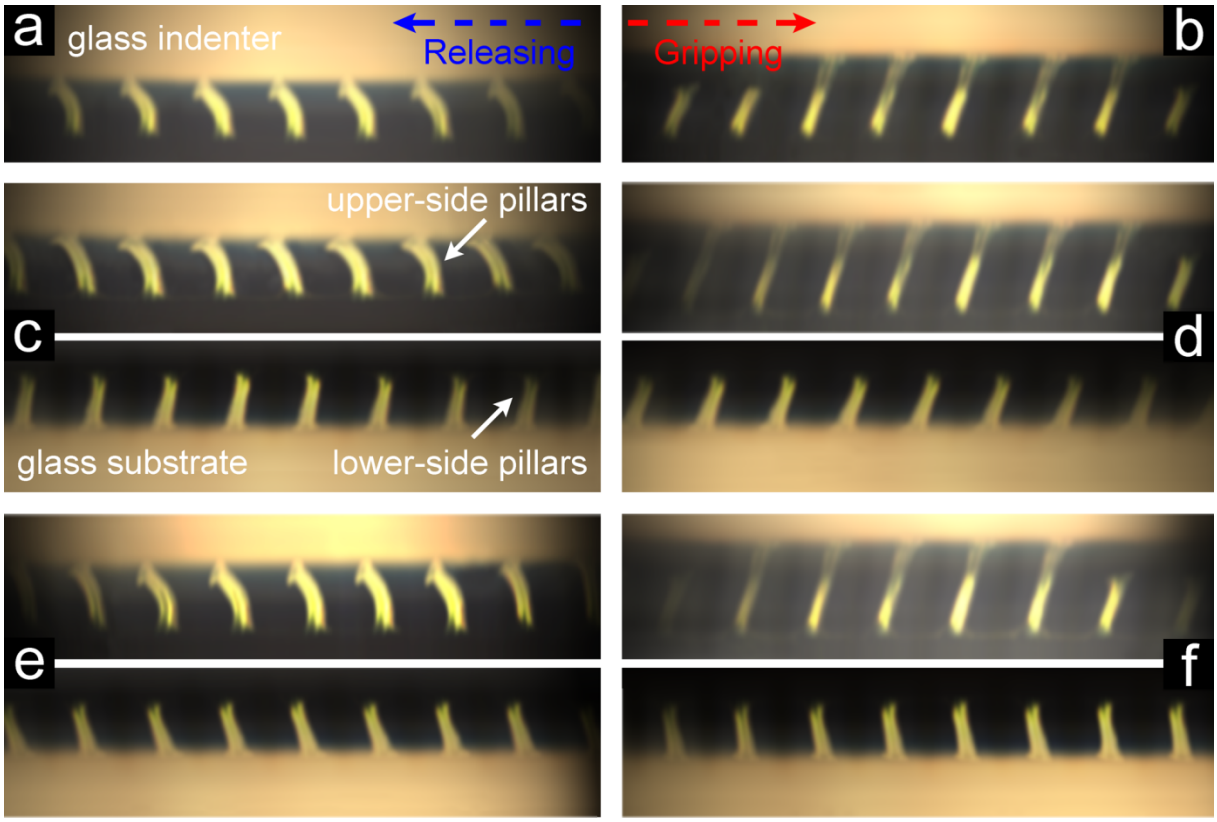


**Fig. S6** Profile view images of the pillar array samples when the maximum adhesive force during retraction is recorded for (a) SSA releasing, (b) SSA gripping, (c) AS-DSA releasing, (d) AS-DSA gripping, (e) S-DSA releasing, and (f) S-DSA gripping. The upper-side and lower-side pillars of DSAs are shown together in the corresponding subgraphs.

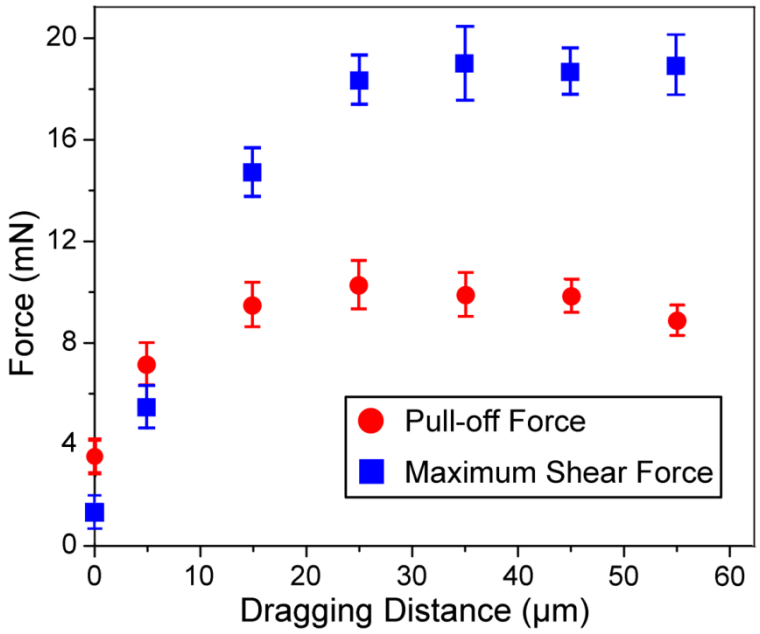


**Fig. S7** Effect of dragging distance on normal and shear adhesion forces in the gripping direction of SSA sample, with fixed dragging velocity of 1 μm $s^{-1}$.

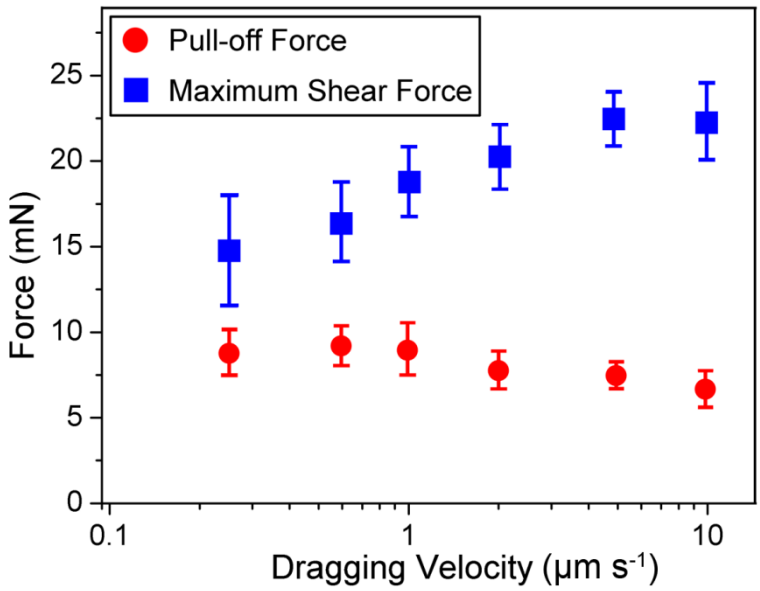


**Fig. S8** Effect of dragging velocity on normal and shear adhesion forces in the gripping direction of SSA sample, with fixed dragging distance of 25 μm.

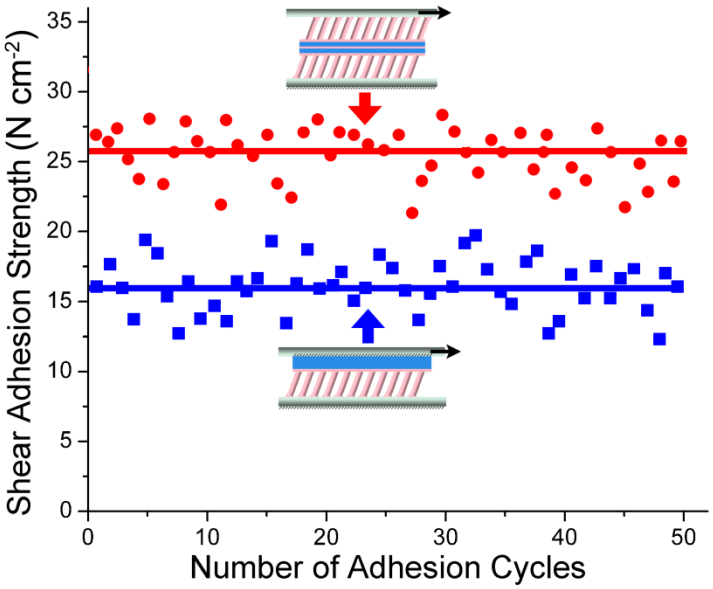


**Fig. S9** Measurements of shear adhesion capacity in the gripping direction of SSA and AS-DSA after 50 cycles of attachment and detachment.

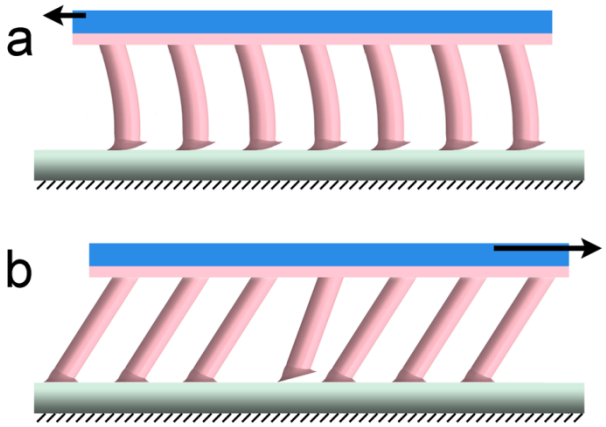


**Fig. S10** Illustration of the pillar-substrate debonding in the conformal shear tests along (a) releasing, and (b) gripping direction, for interpreting the different type of detachment (*i.e.* either instantaneous or gradual).

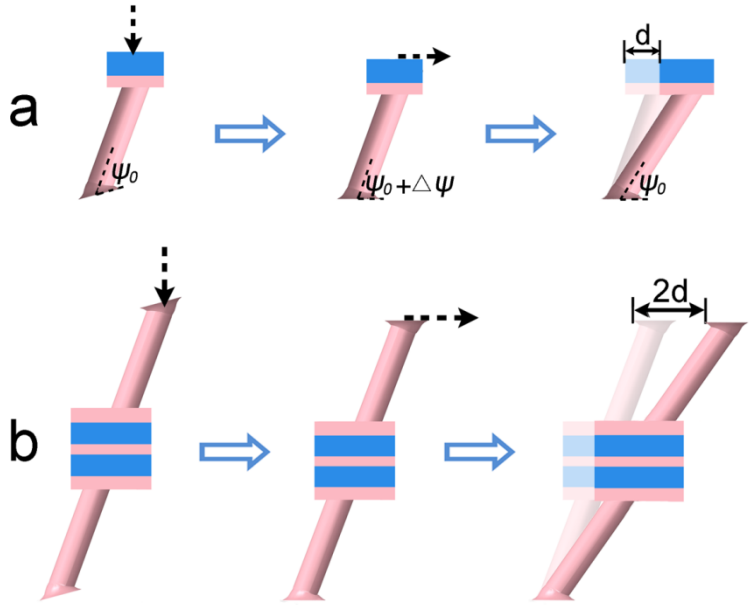


**Fig. S11** Illustration of the allowable shear displacement before detaching from the leading edge (*i.e.* reaching the zero peeling moment limit) of (a) SSA, and (b) AS-DSA in the gripping direction, for interpreting the increased adhesion capacity of AS-DSA compared with SSA.

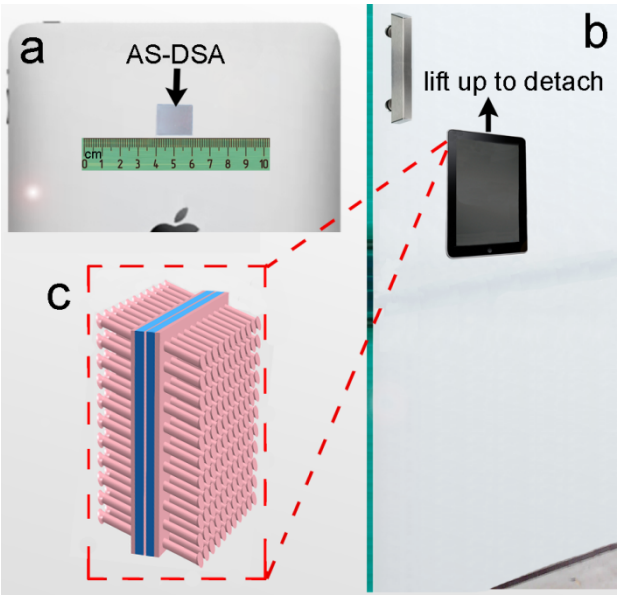


**Fig. S12** Demonstration of applying the AS-DSA sample as a facile fastener for a tablet computer. (a) Photograph of the back side of the tablet computer, where a 2 cm × 2 cm AS-DSA sample is gently attached under a small preload. (b) The computer is fastened on a vertical glass door by the AS-DSA sample, while it can be easily detached by slightly lifting up. (c) Illustration of the pillar alignment of the AS-DSA sample.

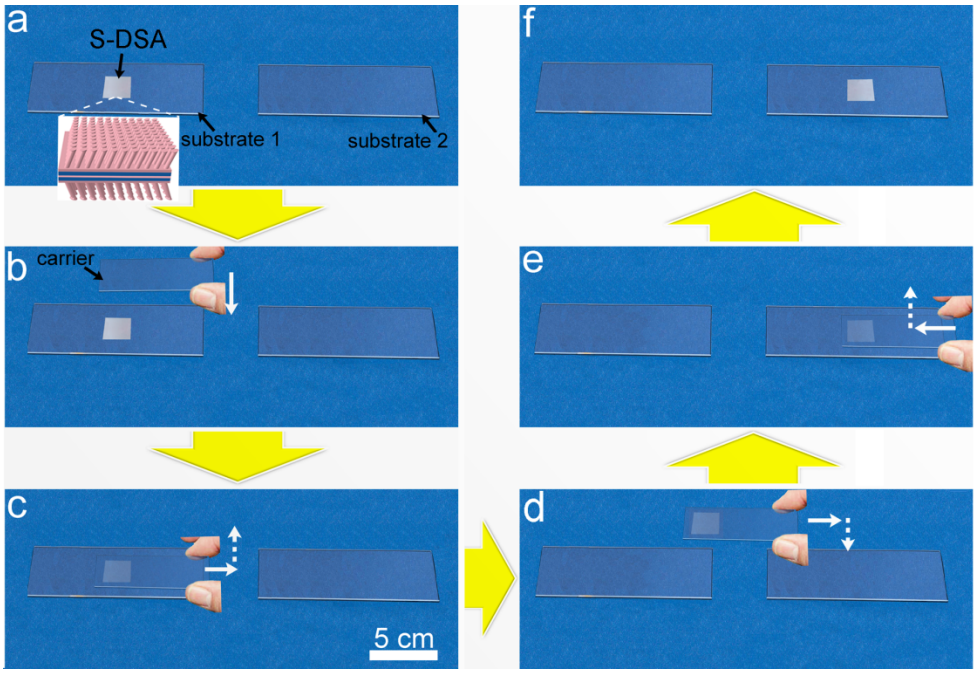


**Fig. S13** Demonstration of the potential application of S-DSA sample in a small-scale delivery setup. (a) The 2 cm × 2 cm S-DSA sample is first attached to one of the two fixed glass substrates under a small preload. (b) A separate glass slide is used as a carrier, for transferring the sample between the two substrates. (c) The carrier is moved into contact with the sample, followed by dragging along the gripping direction of the upper-side pillars. (d) The sample adheres to the carrier after manual separation, due to the releasing effect of the lower-side pillars. (e) The carrier together with the sample is moved into contact with the second substrate, followed by dragging along the gripping direction of the lower-side pillars. (f) The transfer is finished by lifting up the carrier.

Supplementary References

S1 ABAQUS, ABAQUS User's Manual, Version 6.12.

S2 Z. Wang, Y. Xu and P. Gu, *J. Phys. D: Appl. Phys.*, 2012, **45**, 142001.